



Experimental study on temperature fluctuations on plate surface induced by coaxial-jet flow

Xue-Yao Xiong¹ · Zun-Quan Liu¹ · Guo-Yan Zhou¹ · Xing Luo² · Shan-Tung Tu¹

Received: 29 May 2023 / Revised: 5 September 2023 / Accepted: 9 October 2023 / Published online: 9 April 2024

© The Author(s), under exclusive licence to China Science Publishing & Media Ltd. (Science Press), Shanghai Institute of Applied Physics, the Chinese Academy of Sciences, Chinese Nuclear Society 2024

Abstract

In nuclear reactors, temperature fluctuations of fluids may cause fatigue damage to adjacent structures; this is referred to as thermal striping. Research on thermal striping in the upper plenum has mainly focused on fluid fields. Few experimental studies have been reported on solid structures in a fluid field with a coaxial jet. This study entailed an experimental study of the temperature fluctuations in the fluid and on a plate surface caused by a coaxial jet. The temperature fluctuations of the fluid and plate surfaces located at different heights were analyzed. The cause of the temperature fluctuation was analyzed using a transient temperature distribution. The results show that the mixing of the hot and cold fluids gradually becomes uniform in the positive axial direction. The average surface temperatures tended to be consistent. When the jet reaches the plate surface, the swing of the jet center, contraction and expansion of the cold jet, and changes in the jet shape result in temperature fluctuations. The intensity of the temperature fluctuation was affected by the position. More attention should be paid when the plate is located at a lower height, and between the hot and cold-fluid nozzles.

Keywords Temperature fluctuation · Thermal striping · Coaxial jet · Thermal mixing · The upper plenum of nuclear reactor

List of symbols

CHT	Conjugate heat transfer	$a(V_{\text{flowmeter}})$	Half-width of electromagnetic flowmeter (m^3/h)
DSM	Dynamic Smagorinsky model	r	Radius (mm)
IHCP	Inverse heat conduction problem	r_{Cold}	Radius of the cold-fluid inlet (mm)
LES	Large eddy simulation	r^*	Dimensionless radius $r^* = \frac{r}{r_{\text{Cold}}}$
RANS	Reynolds-averaged Navier–Stokes	T	Temperature (K)
RMS	Root mean square	T_{Cold}	Inlet temperature of the cold fluid (K)
SGS	Subgrid-scale	T_{Hot}	Inlet temperature of the hot fluid (K)
URANS	Unsteady Reynolds-averaged Navier–Stokes	T^*	Dimensionless temperature $T^* = \frac{T - T_{\text{Cold}}}{T_{\text{Hot}} - T_{\text{Cold}}}$
$a(T_{\text{Hioki}})$	Half-width of the data acquisition card (K)	T_{Avg}^*	Dimensionless average temperature $T_{\text{Avg}}^* = \frac{1}{n} \sum_{i=1}^n T_i^*$
		T_{RMS}^*	Dimensionless root-mean-square temperature $T_{\text{RMS}}^* = \sqrt{\frac{1}{n} \sum_{i=1}^n (T_i^* - \overline{T^*})^2}$
		t	Time (s)
		$U(T_{\text{thermocouple}})$	Expanded uncertainty of thermocouple (K)
		$u(T_{\text{Hioki}})$	Standard uncertainty of data acquisition card (K)
		$u(T_{\text{thermocouple}})$	Standard uncertainty of thermocouple (K)
		$u(V)$	Standard uncertainty of flow (m^3/h)
		$u(V_{\text{flowmeter}})$	Standard uncertainty of flowmeter (m^3/h)

This work was supported by the National Natural Science Foundation of China (No. 52075173) and the Overseas Expertise Introduction Project for Discipline Innovation (No. B13020).

✉ Guo-Yan Zhou
 zhougy@ecust.edu.cn

¹ Key Laboratory of Pressure Systems and Safety (MOE), East China University of Science and Technology, Shanghai 200237, China

² Institute of Thermodynamics, Gottfried Wilhelm Leibniz University Hannover, 30823 Garbsen, Germany

$u_c(T)$	Combined standard uncertainty of temperature measurement (K) $u_c(T) = \sqrt{u(T_{\text{thermocouple}})^2 + u(T_{\text{Hioki}})^2}$
$u_c(T_{\text{in}})$	Combined standard uncertainty of inlet temperature measurement (K) $u_c(T_{\text{in}}) = \sqrt{\frac{[u(T_{\text{thermocouple}})]^2 + [u(T_{\text{Hioki}})]^2}{3}}$
$u_{\text{crels}}(V)$	Relative expanded uncertainty range of flow $u_{\text{crels}}(V) = k \left(\frac{u_s(V)}{V_{\text{max}}} \frac{u_s(V)}{V_{\text{min}}} \right)$
V	Flow (strip/h)
z_f	Measurement height in the fluid (mm)
z_p	Plate height (mm)
z_f^*	Dimensionless measurement height in the fluid $z_f^* = \frac{z_f}{z_p}$

1 Introduction

During the operation of nuclear reactors, owing to the uneven temperature of fluids, mixing of fluid streams with different temperatures, alternating thermal stress, and severe fatigue damage may occur in adjacent structures [1, 2]. This phenomenon, referred to as thermal striping, is pronounced in the upper plenum of nuclear reactors [3], pipe elbows [4], and T-junction [5]. Elbow failure is often caused by fluid stratification at different temperatures [6]. The causes of thermal striping at the T-junction and upper plenum of nuclear reactors are similar, namely the mixing of fluids at different temperatures [7, 8]. Because temperature change is the main cause of damage, the analysis of temperature fluctuations at the aforementioned locations is the basis for the study of thermal striping [9].

Because T-junctions are a common structure in pipelines, temperature fluctuations in these locations have been extensively studied. At T-junctions, two fluids are mixed vertically at different temperatures. Temperature fluctuations occur downstream of the mixing position [10]. Several studies have been reported on temperature fluctuations in T-junctions. Most such studies have focused on the fluid temperature distribution inside T-junctions under different conditions. Kimura et al. [11] characterized the jet impingement and mixing between a hot stream and a smaller cold branch flow. It was found that the temperature fluctuation in the T-junction with the elbow upstream had a large component at a low frequency compared to the straight case. Zhou et al. [12] conducted thermal mixing experiments to investigate the thermal striping close to a weld connection downstream of a 90° T-junction. The results show that the change in temperature difference has a significant influence on the stability of the thermal stratification in the mixing flow, as well as on the phenomenon of reverse flow. Walker et al. [13] and Kickhofel et al. [14] characterized T-junction mixing

by using wire mesh sensors. The experiments obtained a large amount of temperature distribution data on the cross-section of the T-junction; these data are ideal for verifying the accuracy of the simulation. On the basis of experimental results, many scholars have performed simulation analyses of temperature fluctuations in T-junctions. Most studies indicate that large eddy simulations (LES) can reproduce long-term temperature fluctuations at T-junctions [15, 16]. Qian and Kasahara [17] performed LES analyses of flow and temperature fields at a T-junction by using different subgrid-scale (SGS) models. The simulation results indicate that the numerical schemes significantly affect the temperature distribution and temperature-fluctuation intensity. An approach using the dynamic Smagorinsky model (DSM) and a hybrid scheme with a large blending factor can accurately predict fluid temperature fluctuations. In addition, some studies have focused on the heat transfer between fluids and structures. Guo et al. [18] measured the outer wall temperature and solved one-dimensional and two-dimensional inverse heat conduction problems (IHCPs) to estimate the temperature fluctuations on the inner wall. LES can also be used for the conjugate heat transfer (CHT) analysis between the fluid and pipe wall in a T-junction [19]. Utanohara et al. [20] performed a fluid–structure coupled simulation of a CHT to investigate the predictive performance of the flow and temperature fields and the temperature fluctuation on the inner surface of the pipe at the T-junction. The simulation reproduced the trend of the experimental data, particularly the velocity fluctuation intensity peak near the wall. Although the mixing form of the T-junction differs from that of the upper plenum, these studies provide important methodological references for studying the temperature fluctuations in the upper plenum.

In the upper plenum, owing to the distribution characteristics of the core assemblies, there were many fuel assemblies around each control-rod assembly at different distances. Moreover, the coolant flow in each channel around the fuel assembly is not always consistent. This led to different coolant temperature profiles in each channel, resulting in thermal striping. In the upper plenum, multiple fluids of different temperatures flow and mix in parallel, causing temperature fluctuations in the flow direction [21]. Thermal striping in the upper plenum damages many vital components. Therefore, they have attracted significant attention [22]. Over the past few decades, various thermal striping studies focusing on the upper plenum of nuclear reactors have been reported. The upper plenum was previously simplified as a parallel jet model. Wakamatsu et al. [23] conducted an experimental study on thermal striping in an upper plenum. In their study, a parallel jet model was adopted to analyze the attenuation characteristics of temperature fluctuations with water and liquid sodium, and a general attenuation range was provided. Tokuhiko et al. [1] further investigated thermal striping by

using a triple parallel jet model. The mixing locations were measured and determined using the same velocities and various velocity cases. Chacko et al. [24] conducted a numerical study by using a triple parallel jet. It was found that LES could be used to analyze the unsteady characteristics of thermal striping. Their study also indicated the limitations of the Reynolds-averaged Navier–Stokes (RANS) approach for unsteady heat transfer simulations. Wang et al. [25, 26] used LES to study the temperature fluctuations caused by a parallel jet in different media. They concluded that the temperature-fluctuation amplitudes of the lead-based materials were more significant than those of sodium. Yu et al. [27] conducted steady and unsteady simulations (RANS, unsteady RANS (URANS), and LES) based on the triple parallel jet model. The temperature fluctuation in the unsteady simulation agreed well with the experimental results. Lomperski et al. [28] presented velocity and temperature field measurements in which two air jets were mixed and impinged on a wall. This indicates that the mixing is better when the jet impacts the wall than when it is freely extended. Krishna et al. [29] employed two parallel jets impinging on a lattice plate above them. The Reynolds stress turbulence model was used to evaluate temperature fluctuations near the plate. Jets with a unity velocity ratio exhibited the maximum temperature fluctuations. Kimura et al. [30] employed a triple parallel jet to experimentally investigate the transfer characteristics of temperature fluctuation from the fluid to the structure. The nonstationary heat transfer characteristics can be represented by a heat transfer coefficient that is constant in time and independent of the frequency of the temperature fluctuation. The aforesaid studies analyzed the thermal striping phenomenon by using parallel jet and triple parallel jet models, which can reflect the two-dimensional characteristics of the temperature fluctuations. However, the thermal mixing in the upper plenum is a complex phenomenon. Thermal striping exhibits strong three-dimensional characteristics at this location.

Consequently, many studies have simplified the upper plenum of nuclear reactors to a coaxial-jet model. Because coaxial jets can reflect the three-dimensional characteristics of temperature fluctuations, their use to describe the thermal striping phenomenon is reasonable [31]. Lu et al. [32] conducted coaxial-jet experiments to investigate the temperature-fluctuation characteristics of a flow field. They found that the alternating extrusion of hot and cold flow columns caused temperature fluctuations. Koket al. [33] experimentally and numerically investigated the mixing behavior of hot and cold fluids for coaxial-jet flows. The thermal mixing efficiency increased with the temperature difference between the hot and cold jet flows. The thermal mixing performance was improved by increasing the hot-jet flow rate. Tenchine et al. [34] conducted jet experiments on sodium and air. The objective of their

experiment was to evaluate the possibilities and limitations of simulating sodium-mixing jets by using a typical fluid. It was found that a rather good estimation of the mean sodium temperature and temperature fluctuation was possible when tests using a simulant fluid were performed at a Reynolds number close to that of the prototype. Their study on the temperature fluctuation induced by a coaxial jet was limited to the fluid field. The swing of the jet likely causes a constant change in the fluid temperature at some positions. However, this change is also transferred to the adjacent solid structures, resulting in temperature fluctuations in solid structures. However, the plate in the fluid causes the flow field to change. Therefore, to elucidate the mechanism of thermal striping, the temperature fluctuations of the flow field and structure surface caused by coaxial-jet flows with an adjacent solid structure must be experimentally examined.

In this study, the thermal striping phenomenon induced by a coaxial jet was experimentally investigated using a coaxial-jet experimental setup. The temperature fluctuations of the fluid and plate surfaces in the coaxial-jet flow field were examined. The transient temperatures of the plates located at different heights were measured and analyzed. Subsequently, variations in the average temperature and local temperature-fluctuation intensity along the axial direction were studied.

2 Experimental setup

2.1 System description

An experimental setup based on a coaxial-jet model was designed and built to study the temperature fluctuations. The setup included hot fluid, cold fluid, mixing, and measurement systems, as shown in Fig. 1a. Both hot- and cold-fluid systems consist of a thermostatic water tank, booster pump, electromagnetic flowmeter, storage tank, valves, and pipes, which can provide steady water flow at specified temperatures and flow rates. The mixing system included coaxial-jet nozzles, a mixing zone, valves, and pipes. The coaxial-jet nozzle was designed using two independent passages. Cold fluid flows through the central passage, whereas hot fluid flows through the outer passage. The two fluids are mixed coaxially in the mixing zone. The measurement system is mainly used for the temperature measurement of the fluid and plate surface in the mixing zone and comprises thermocouples, brackets, a data acquisition card, and a computer.

During the experiment, hot and cold water were pumped into the mixing zone from the thermostatic water tank via the valves. The mixed water flows into the storage tank and then recycled into the thermostatic water tank. Figure 1b shows a photograph of the experimental setup.

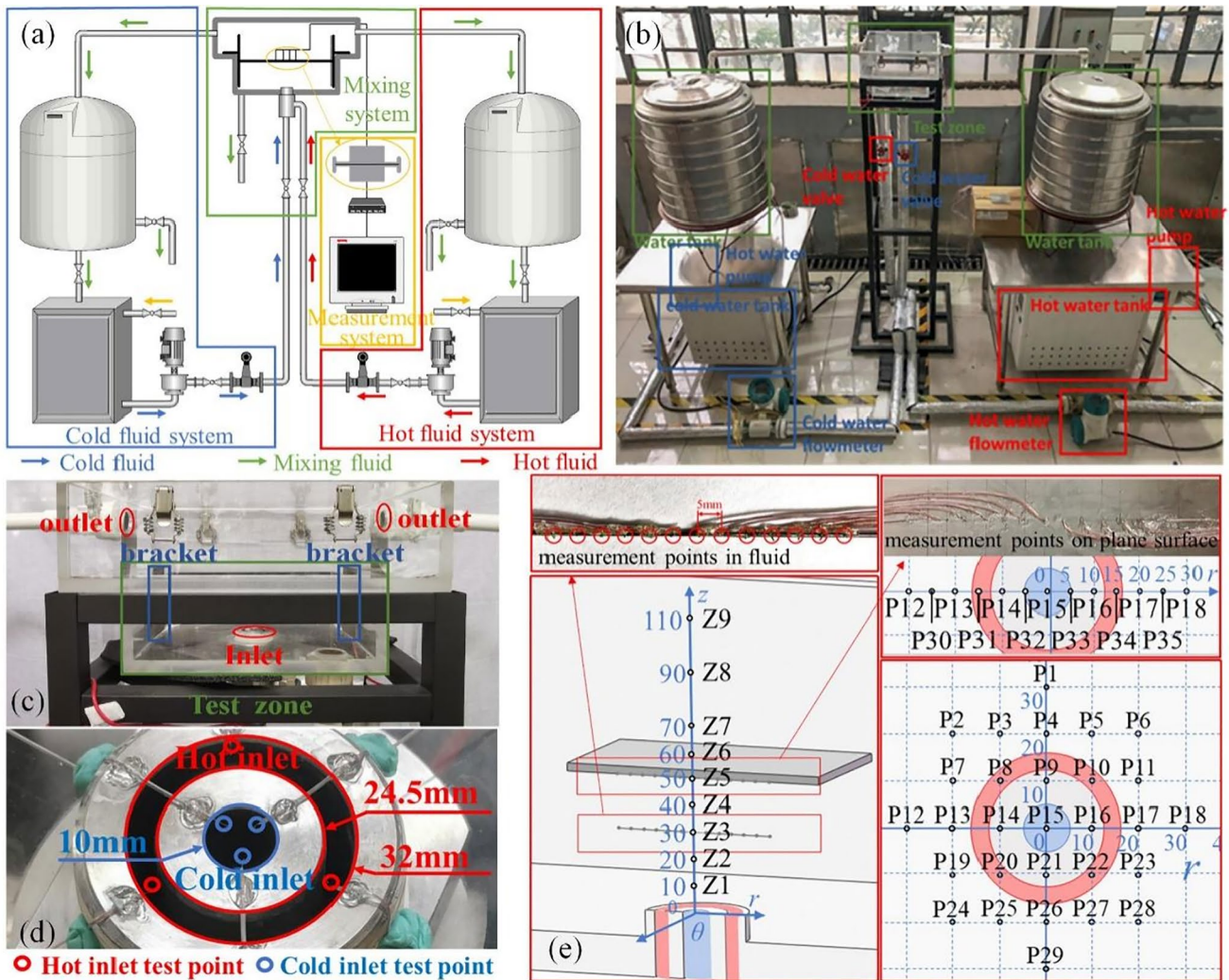


Fig. 1 (Color online) Experimental setup and measurement points. **a** Schematic of the experimental setup **b** Photograph of the experimental setup **c** Test zone **d** Coaxial-jet nozzle **e** Schematic of measurement points

2.2 Test zone and inlet temperature test point

The test zone was a transparent acrylic box with dimensions 250 mm × 250 mm × 100 mm, as shown in Fig. 1c. The coaxial jet inlet is located at the bottom of the test zone. The nozzle was placed 10 mm above the bottom to reduce the impact of the bottom plate on the inlet fluid. The outlet was located on the two sides above the box, away from the test zone, to reduce its impact on the flow field. The brackets were movable and can be placed at certain heights within the box to enable temperature measurements at different heights.

The cold-fluid inlet was circular with a diameter of 10 mm. The hot fluid inlets were annular with 24.5 and 32 mm. Three measurement points were evenly arranged on the circumferences of the hot and cold-fluid nozzles to measure the inlet temperatures of the fluids, as shown in Fig. 1d.

2.3 Uncertainty analysis

The temperature was measured using a T-type thermocouple with a diameter of 0.08 mm. The time interval for temperature sampling was 0.01 s. The velocity was calculated using the hot and cold flow rates and the cross-sectional area of the coaxial-jet nozzle. The hot and cold flow rates were measured using electromagnetic flow meters. The setup temperature measurement range was 20–90 °C, and the flow rate was 0.141–2.802 m³/h. The temperature measurement uncertainty was determined using a thermocouple and a data acquisition card. An electromagnetic flow meter was used to directly determine the uncertainty in the flow measurement.

The measurement range and accuracy of the equipment were as follows. The measurement range of the T-type thermocouple was 0–150 °C, and the expanded uncertainty was $U(T_{\text{thermocouple}}) = 0.2$ K with an inclusion

factor $k=2$. The standard uncertainty of the thermocouple $u(T_{\text{thermocouple}})=0.1$ K. The interval half-width of the data acquisition card (model, Hioki) $a(T_{\text{Hioki}})=0.5$ K for the T-type thermocouple within 0–100 °C. The electromagnetic flowmeter measurement range was 0–3 m³/h with a half-width $a(V_{\text{flowmeter}})=0.0102$ m³/h. Considering uniform distribution, the inclusion factor was taken as $k=\sqrt{3}$, and the standard uncertainty of the data acquisition card $u(T_{\text{Hioki}})=0.28$ K. The standard uncertainty of flowmeter $u(V_{\text{flowmeter}})=0.00589$ m³/h. The combined standard uncertainty of the temperature measurement $u_c(T)$ can be obtained using Eq. (1) [35].

$$u_c(T) = \sqrt{u(T_{\text{thermocouple}})^2 + u(T_{\text{Hioki}})^2} \tag{1}$$

Thus, the combined standard uncertainty of the temperature $u_c(T) = 0.311$ K. Similarly, the standard uncertainty $u(V)$ and relative expanded uncertainty range $u_{\text{crels}}(V)$ of the flow measurement can be obtained using Eqs. (2) and (3), respectively:

$$u(V) = u(V_{\text{flowmeter}}), \tag{2}$$

$$u_{\text{crels}}(V) = k \left(\frac{u_s(V)}{V_{\text{max}}} \sim \frac{u_s(V)}{V_{\text{min}}} \right). \tag{3}$$

The standard uncertainty $u(V) = 0.00589$ m³/h, and the expanded uncertainties of the flow measurement $u_{\text{crels}}(V) = 0.42$ –8.4%.

The inlet temperature T_{in} is the average of the values at the three measurement points.

The combined standard uncertainty of the inlet temperature measurement $u_c(T_{\text{in}})$ can be calculated using Eq. (4).

$$u_c(T_{\text{in}}) = \sqrt{\frac{[u(T_{\text{thermocouple}})]^2 + [u(T_{\text{Hioki}})]^2}{3}} \tag{4}$$

The combined uncertainty of inlet temperature measurement $u_c(T_{\text{in}})$ was 0.180 K. This shows that the setup has high measurement stability and can be used for experimental measurements.

2.4 Data processing method

For the convenience of discussion, the temperature and radius values were nondimensionalized. The dimensionless temperature is expressed as

$$T^* = \frac{T - T_{\text{Cold}}}{T_{\text{Hot}} - T_{\text{Cold}}}, \tag{5}$$

where T_{Cold} and T_{Hot} denote the inlet temperatures of the cold and hot fluids, respectively. The average values measured

at the test points at the inlet were used. The dimensionless average temperature was calculated as

$$T^*_{\text{Avg}} = \frac{1}{n} \sum_{i=1}^n T^*. \tag{6}$$

The dimensionless radius is the ratio of the diameter to the cold-fluid inlet diameter.

$$r^* = \frac{r}{r_{\text{Cold}}} \tag{7}$$

where r_{Cold} is the radius of the cold-fluid inlet (5 mm). The root-mean-square (RMS) temperature can be used to express the intensity of temperature fluctuations.

$$T^*_{\text{RMS}} = \sqrt{\frac{1}{n} \sum_{i=1}^n (T^*_i - \bar{T}^*)^2} \tag{8}$$

3 Coaxial-jet experiment scheme

The temperature sensors were fixed in the fluid and on the plate surface using detachable brackets. The temperature measurements of the plate surface were divided into two parts. First, the 29 points shown in Fig. 1e were arranged to measure the entire plane of the lower surface. Because the temperature fluctuation caused by the coaxial jet was symmetrical, the measurement points were arranged along the radial direction in further tests. There were 13 measurement positions on the plate surface, as shown in Fig. 1e, at which the thermocouples were pasted without covering so that the thermocouple can be in contact with the fluid. To measure the fluid temperature, 13 thermocouples were fixed on a tungsten steel wire under the plate surface, as shown in Fig. 1e. The measurement point positions were the same as those shown in Fig. 1e.

The plate size was 100 mm × 100 mm, and the thickness was 1 mm. Its material is stainless steel 316, with a density of 7.98 g/cm³, thermal conductivity of 15.1 W/(m·K), and specific heat capacity of 0.502 J/(g·K).

For all the test cases, the flow velocity was 0.5 m/s. The plate height z_p was varied from 30 to 110 mm. The cold and hot water temperatures were set at 20 and 40 °C, respectively. The thermocouple sampling time interval was 0.01 s, and the measurement time of a single test was approximately 180 s. The experimental conditions are listed in Table 1.

4 Temperature fluctuation on the plate surface

Considering a plate height of 50 mm as an example, in addition to the temperature fluctuations on the plate surface, the fluid temperature fluctuation between the coaxial-jet nozzle

Table 1 Experiment conditions

		Height (mm)	Hot water		Cold water	
			Temperature (°C)	Velocity (m/s)	Temperature (°C)	Velocity (m/s)
Plate surface	Case 1	30	40	0.5	20	0.5
	Case 2	40	40	0.5	20	0.5
	Case 3	50	40	0.5	20	0.5
	Case 4	60	40	0.5	20	0.5
Fluid in radial direction	Case 5	10	40	0.5	20	0.5
	Case 6	20	40	0.5	20	0.5
	Case 7	30	40	0.5	20	0.5
	Case 8	40	40	0.5	20	0.5
Plate surface in the radial direction	Case 9	30	40	0.5	20	0.5
	Case 10	40	40	0.5	20	0.5
	Case 11	50	40	0.5	20	0.5
	Case 12	70	40	0.5	20	0.5
	Case 13	90	40	0.5	20	0.5
	Case 14	110	40	0.5	20	0.5

and the plate was analyzed. The height measurement range for the fluid temperature was 10–40 mm, shown as by Z1–Z4 in Fig. 1e. The dimensionless heights were calculated as

$$z_f^* = \frac{z_f}{z_p}, \quad (9)$$

where z_f is the measured height of the fluid. z_p is the plate height, which was 50 mm in this study.

4.1 Transient temperature analysis

Subsequent average temperature analysis revealed that the dimensionless average temperature of the fluid was symmetric. Therefore, an analysis of the transient temperature was performed along the radius (P15–P18 in Fig. 1e). The temperature fluctuations were entirely random, as shown in Fig. 2a. When the plate height $z_p = 50$ mm, the temperature at each radial position significantly fluctuated; $r^* = 0$ showed the most pronounced fluctuations. In addition, there were small fluctuations overall temperature increase and decrease. For example, at $r^* = 0$, the temperature shows a decreasing trend between 0 and 0.2 s; however, this process is accompanied by two minor temperature increases.

The cause of the temperature fluctuation can be analyzed by comparing the temperature fluctuation in Fig. 2a with the transient temperature distribution on the plate surface at different times shown in Fig. 3a. These temperature fluctuations can mainly be attributed to the fluid instability. As indicated by the transient temperature distribution on the plate structure, this instability is mainly reflected in the following three aspects. First, the cold fluid would expand

and contract as time progresses. For example, the cold fluid expands during 0–0.2 s and contracts during 0.2–0.4 s. Correspondingly, the center ($r^* = 0$) temperature decreases in 0–0.2 s, and the temperature increases in 0.2–0.4 s (Fig. 2a). Second, the jet center would swing over time. At 0.2 s, the center of the cold fluid was at $r^* = 0$, as shown in Fig. 3a. At 0.5 s, the center moved downward. At 0.6–0.7 s, the cold-fluid center appeared on the left. The transient temperatures are presented in Fig. 2a. The temperature at $r^* = 2$ increases when the cold-fluid center swings to the left at 0.4 s. Finally, the shape of the jet also changes significantly. Occasionally, the temperature distribution on the plate surface presents a relatively regular circle, for instance, that at 1.1 s. It may also extend in different directions, for example, the observations corresponding to 0.1 s, 0.2 s, and 0.9 s. Mostly, the shape of the jet is relatively irregular. Under the combined influence of these three factors, the temperature would fluctuate at each point on the plate surface.

In the flow field between the jet nozzle and the plate, the transient temperatures at $z_f^* = 0.2$ and $z_f^* = 0.6$ were as shown in Fig. 2b. The position at which the temperature fluctuation is relatively prominent changes along the axial direction. The position with notably evident temperature fluctuation is at $r^* = 1$ when $z_f^* = 0.2$ and at $r^* = 0$ when $z_f^* = 0.6$. Compared to plate surface, temperature changes were more frequent in the flow field $z_f^* = 0.2$ and $z_f^* = 0.6$.

4.2 Average temperature distribution

Over a long period, the temperatures at various radial positions fluctuated around a fixed value. This is reflected in the dimensionless average temperature values. The

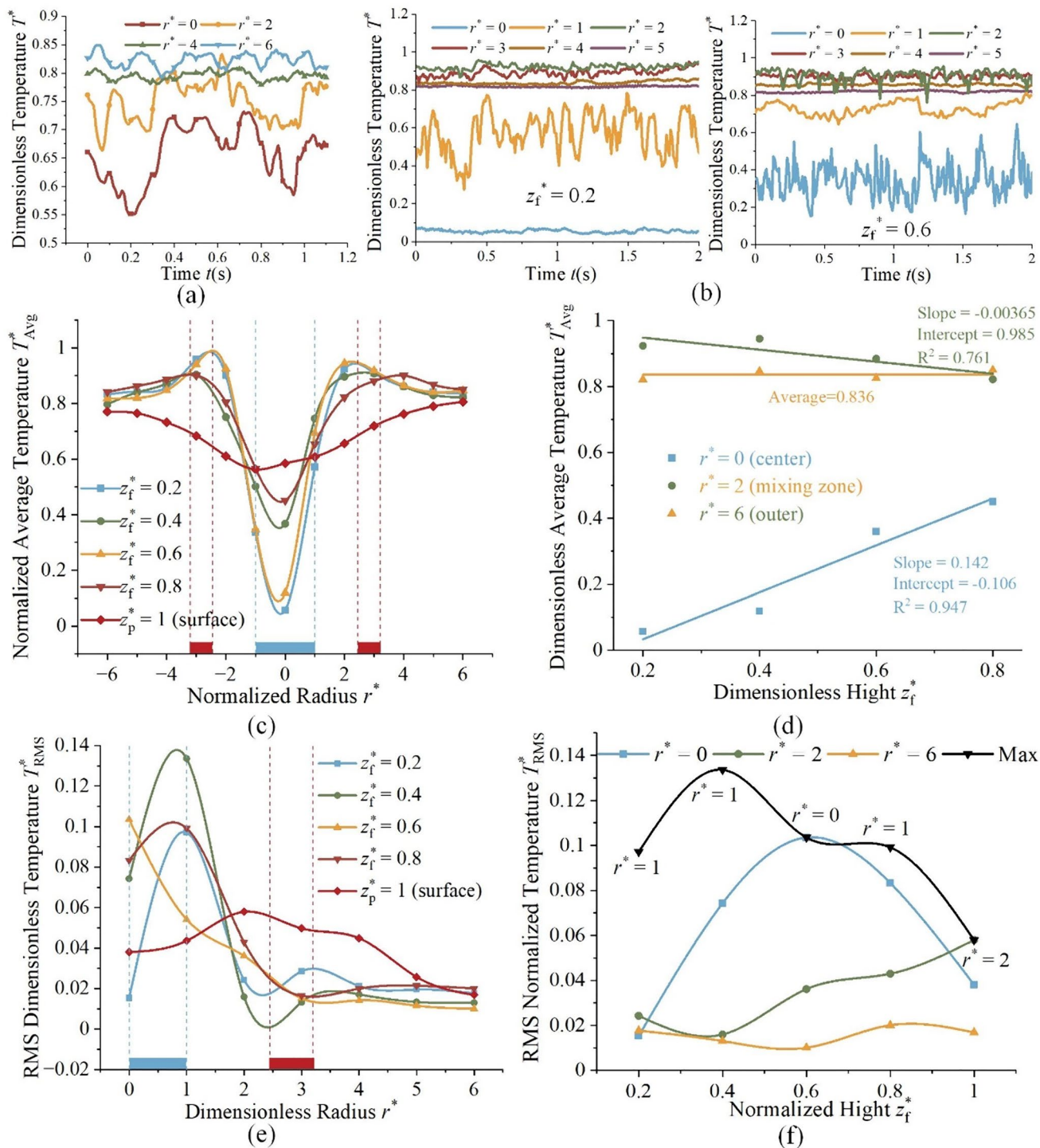


Fig. 2 (Color online) Dimensionless transient temperature, average temperature, and intensity of temperature fluctuations of fluid on the plate surface **a** Transient temperature on plate surface with plate height $z_p = 50$ mm **b** Transient temperature of fluid with plate height

$z_p = 50$ mm **c** Average temperature in the radial direction **d** Average temperature in the axial direction **e** RMS temperature in the radial direction **f** RMS temperature in the axial direction

dimensionless average temperature of the plate surface at $z_p = 50$ mm is shown in Fig. 4a. The average temperature was the lowest at the center and continued to increase along

the radial direction. The temperature distribution was almost circular. Therefore, the temperature along the radial direction was selected for further analysis. The dimensionless

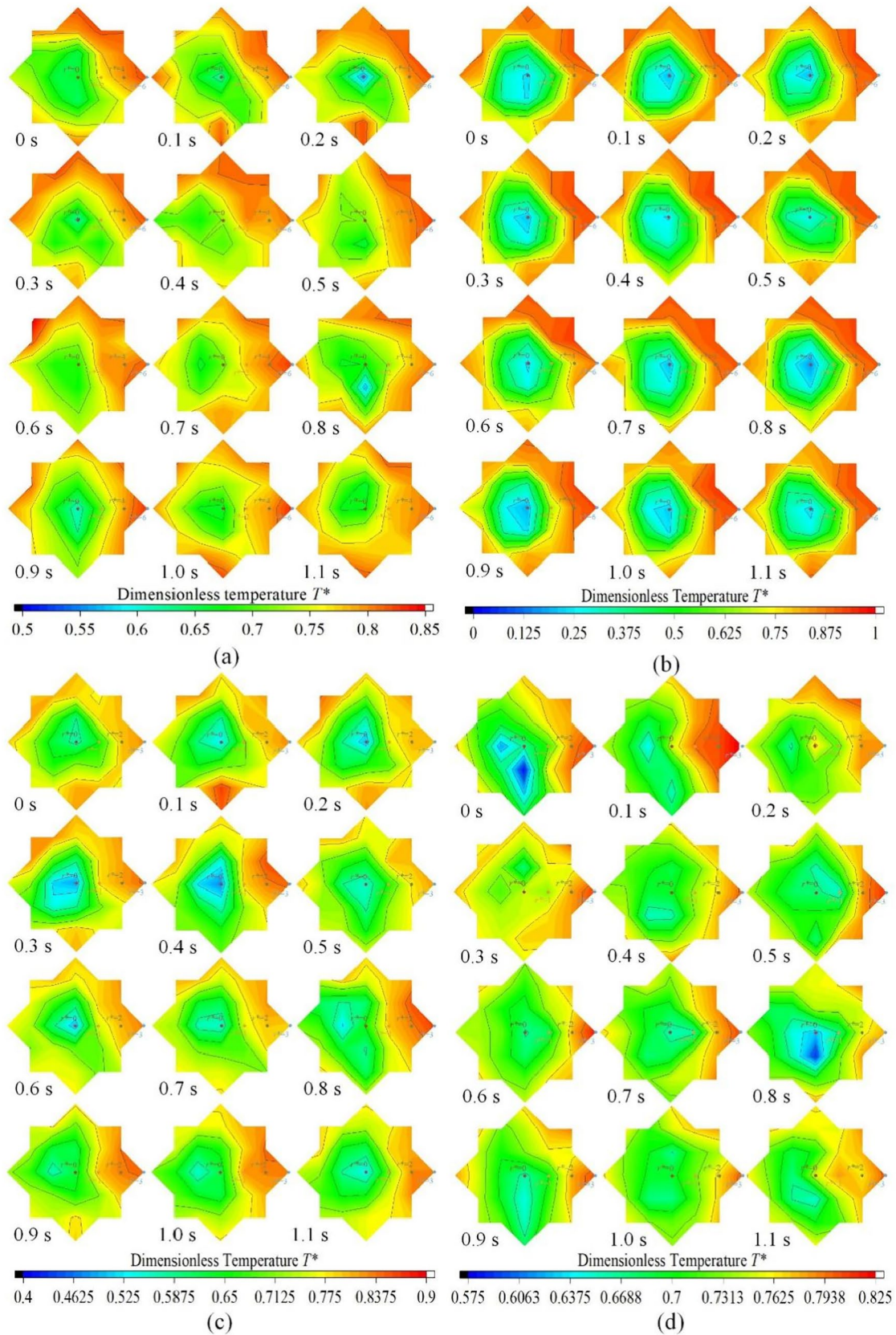


Fig. 3 (Color online) Dimensionless transient temperature distribution on the plate surface **a** $z_p = 50$ mm **b** $z_p = 30$ mm **c** $z_p = 40$ mm **d** $z_p = 60$ mm

average temperature of the fluid in the radial direction was symmetrical, as shown in Fig. 2c. The blue and red blocks on the horizontal axis represent the positions of the cold and hot fluid nozzles, respectively. The average temperature was the lowest at the center. In the positive radial direction, it increased rapidly and reached the maximum value above the hot fluid nozzle. Subsequently, the average temperature decreased slowly and finally reached a constant value of approximately 0.836. Moreover, the lower the height, the smaller would be the minimum value and the larger would be the maximum value. The average dimensionless temperature on the plate surface showed a considerably different behavior. It increased continuously in the positive radial direction. There was no longer a prominent high-temperature peak above the hot fluid nozzle. This phenomenon may be attributed to the cold fluid in the center flowing in all directions and rapidly mixing with the hot fluid when the jet reaches the plate surface.

To examine the temperature variation in the axial direction, the center position (P15 in Fig. 1e, $r^* = 0$), mixing zone between the hot and cold fluids (P16 in Fig. 1e, $r^* = 2$), and outer position (P18 in Fig. 1e, $r^* = 6$) were considered for the analysis. Figure 2d shows the average dimensionless temperature of the fluid in the axial direction. The average temperature increased at the center ($r^* = 0$) in the axial direction. It decreases at $r^* = 2$ and remains constant at $r^* = 6$. This variation is linear between $z_f^* = 0.2$ – 0.8 .

4.3 Intensity of temperature fluctuation

Intensity of the temperature fluctuations can better characterize their severity. This can be expressed as the RMS temperature. For $z_p = 50$ mm, the RMS dimensionless temperature on the plate surface was as shown in Fig. 4b. The temperature evidently fluctuated above the jet nozzle. The RMS temperature along the radial direction is shown in Fig. 2e. At $z_f^* = 0.2, 0.4,$ and 0.8 , the RMS temperature initially increased and then decreased, with the maximum value observed at $r^* = 1$. At $z_f^* = 0.6$, the RMS temperature decreased continuously from $r^* = 0$. At the plate surface, the RMS temperature was relatively higher in the range of $r^* < 4$.

Figure 2f shows the variation of the intensity of the temperature fluctuations in the axial direction. At $r^* = 0$, the RMS temperature increased when $z_f^* < 0.6$ and gradually decreases when $z_f^* \geq 0.6$. It shows an increasing trend at $r^* = 2$ and remains constant at $r^* = 6$. Severe temperature fluctuations indicated that the hot and cold fluids constantly alternated at this position. This point was the junction of the hot and cold fluids. Therefore, the intensity of the temperature fluctuation at $r^* = 0$ reflected the amplitude of the jet swing. When $z_f^* < 0.6$, the jet swing amplitude increased in the axial direction. The junction between the hot and cold fluids can swing toward the center. Therefore, the RMS

temperature at $r^* = 0$ continued to increase. When $z_f^* \geq 0.6$, the plate makes the jet more stable, and the swing amplitude becomes small. The RMS temperature decreases at $r^* = 0$. This phenomenon was also reflected in the maximum RMS temperature, as shown in Fig. 2f. When $z_f^* < 0.6$, the maximum RMS temperature was observed at $r^* = 1$. With increasing height, it moved to the center ($r^* = 0$). Evidently, the RMS temperature is the highest at $r^* = 0$ when $z_f^* = 0.6$ in Fig. 2f. When the position approaches the plate surface, the maximum RMS temperature was restored to $r^* = 1$ at $z_f^* = 0.8$. In the flow field, hot and cold fluid flowed along the positive axial direction. When the fluid reached the plate surface, the direction of fluid flow changed. The fluid flowed along the radial directions. Therefore, the junction of the cold and hot fluids moves outward. The maximum RMS temperature was observed at $r^* = 2$ on the plate surface. Furthermore, the maximum RMS temperature at the position $0.2 < z_f^* < 0.8$ is much larger than that on the plate surface; this implies that the temperature-fluctuation attenuation is rapid near the plate surface.

5 Effect of plate height on temperature fluctuation

To experimentally investigate the effect of plate height, the plate was placed above the jet nozzle at different heights, and the temperature fluctuations on the lower surface were measured. The height range was 30–110 mm, denoted as Z3–Z9 in Fig. 1e.

5.1 Transient temperature changes with height

Compared with $z_p = 50$ mm, the cold fluid expanded and contracted with time at different plate heights. However, changes in the swing and shape of the jet were insignificant when the plate height $z_p = 30$ mm. As the height increases, the jet swing and temperature distribution changes become increasingly pronounced, as shown in Fig. 3.

The transient temperature at $z_p = 30$ mm and its frequency domain representation in the radial direction are shown in Fig. 5. The temperature fluctuation was the most severe at $r^* = 2$ between the hot and cold fluids at this height. The fluctuation range was approximately 0.2–0.9. The frequency domain (Fig. 5a) representation shows that the temperature fluctuation has no prominent peak frequency. However, the temperature fluctuations were more severe at lower frequencies. At $r^* = 2$, the frequency of the temperature fluctuation was mainly distributed within 10 Hz. At $r^* = 0$, the amplitude above 5 Hz is almost zero.

The transient temperature variations at plate heights $z_p = 40, 50, 70,$ and 90 mm are shown in Fig. 5. The ranges of temperature fluctuations at different positions

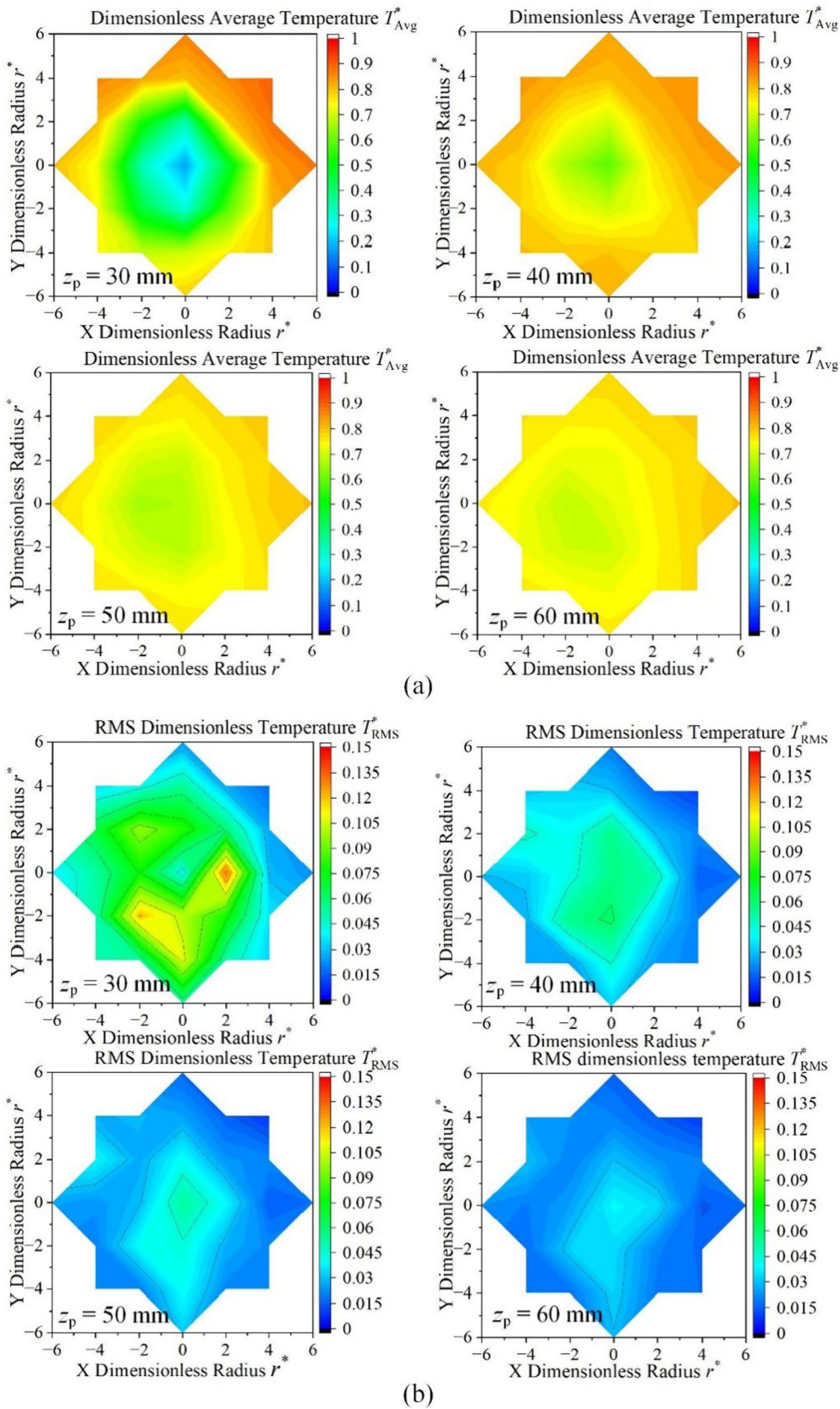


Fig. 4 (Color online) Dimensionless average temperature and RMS dimensionless temperature on the plate surface **a** Average temperature **b** RMS temperature

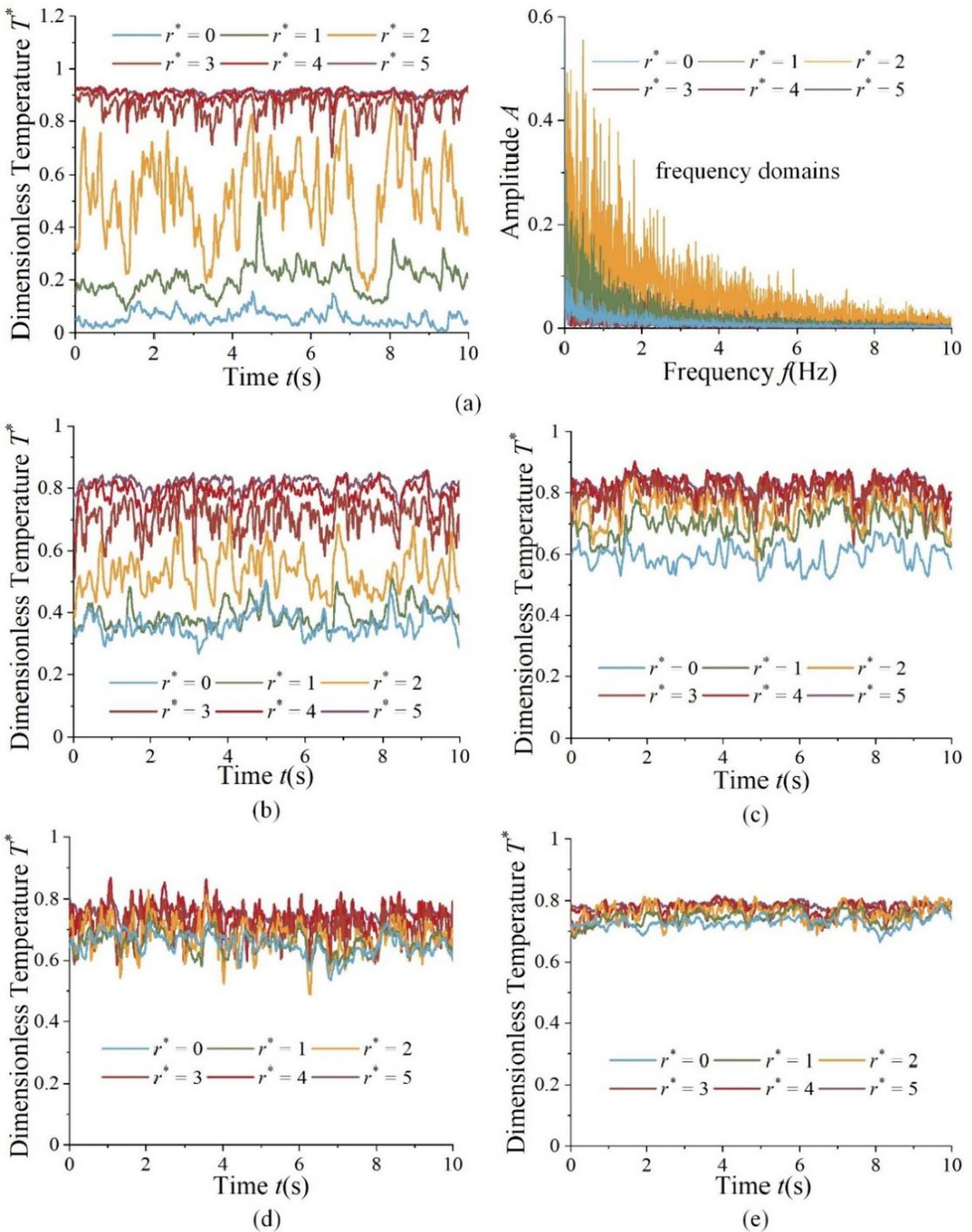


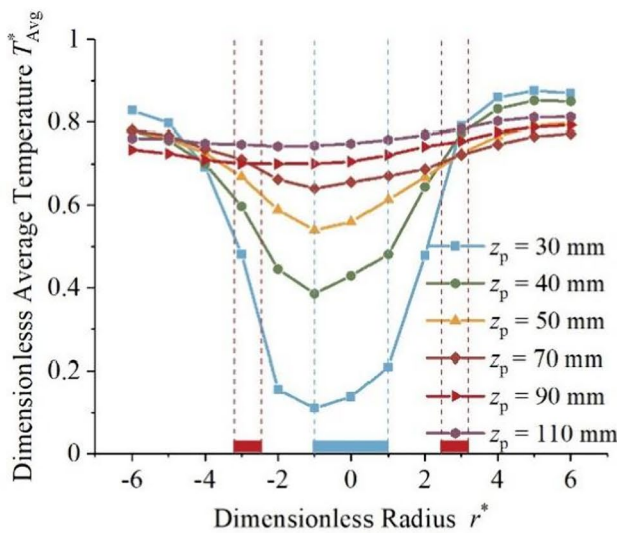
Fig. 5 (Color online) Transient dimensionless temperature in time and frequency domains **a** $z_p = 30$ mm **b** $z_p = 40$ mm **c** $z_p = 50$ mm **d** $z_p = 70$ mm **e** $z_p = 90$ mm

exhibited different changes in the axial direction. At the center ($r^* = 0$), the temperature-fluctuation range changed from 0–0.1 at $z_p = 30$ mm to 0.5–0.7 at $z_p = 50$ mm and 0.7–0.8 at $z_p = 90$ mm. The temperature-fluctuation range at $r^* = 2$ decreased from 0.2–0.9 at $z_p = 30$ mm to 0.7–0.8 at $z_p = 90$ mm. The temperature fluctuation at $r^* = 5$ was from 0.9–1 at $z_p = 30$ mm to 0.75–0.85 at $z_p = 50$ mm and finally reached 0.7–0.8 at $z_p = 90$ mm. During the entire process, the fluctuation range remained almost unchanged. Only the average temperature decreased slightly. The variation in the temperature-fluctuation range was the result of cold and hot fluids mixing and jet instability. The variation in temperature fluctuation with height was analyzed using the average temperature and temperature fluctuation intensity.

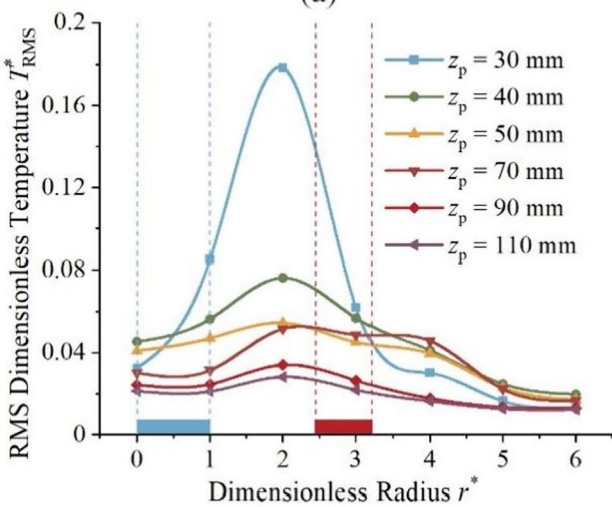
5.2 Average temperature changes with height

The average temperature of the center gradually increased in the positive axial direction. The outside temperature gradually decreased, as shown in Fig. 4a. The temperature distribution was almost circular. Therefore, the temperature in the radial direction was used for further analysis.

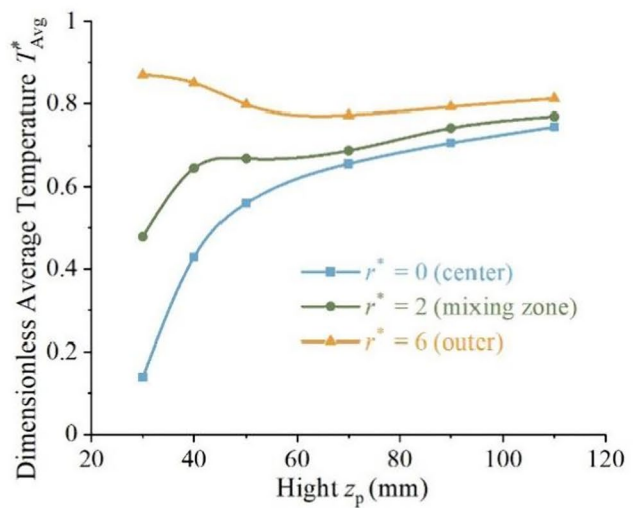
The dimensionless average temperature of the plate surface in the radial direction is shown in Fig. 6a. The temperature in the radial direction was symmetrical. However, because of the non-coaxial nature of the testing bracket, its symmetry region was between $r^* = 0$ and $r^* = -1$. The average temperature at the center was low and increased gradually with the radius. It reached a constant value at $r^* = 5$. As



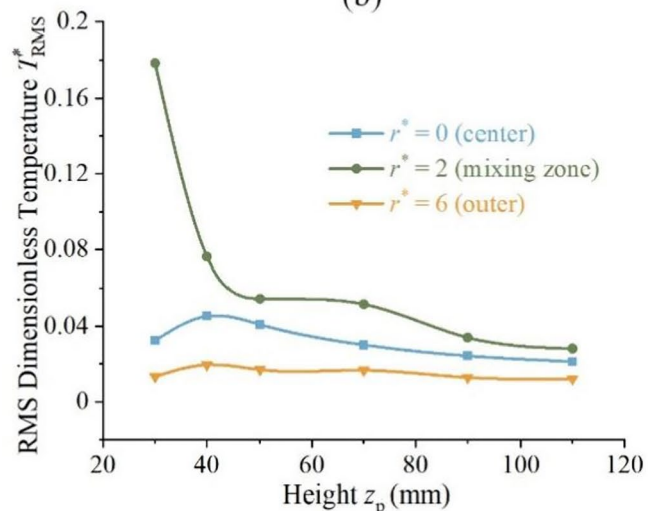
(a)



(c)



(b)



(d)

Fig. 6 (Color online) Dimensionless average temperature and intensity of temperature fluctuations on the plate surface **a** Average temperature in the radial direction **b** Average temperature in the axial

direction **c** RMS temperature in the radial direction **d** RMS temperature in the axial direction

the height increased, the temperature at the center increased. The temperature at each radial point was identical. This indicated that the mixture became uniform.

The dimensionless average temperature variation along the axial direction was as shown in Fig. 6b. The temperature at $r^* = 0$ increased continuously with increasing height. The position at $r^* = 2$ showed a relatively slow increase. However, the temperature at $r^* = 6$ decreases in the range of $30 < z_p \leq 70$ mm. When $z_p > 70$, it remained almost constant. This demonstrates the effect of height on fluid mixing. At $z_p = 30$ mm, the average temperature at $r^* = 0$ is approximately 0. This implies that the cold fluid at the center did not start to mix. The temperature at each point changed rapidly within the range $30 < z_p \leq 70$ mm. This implies that the fluid mixes rapidly at this height. When $z_p > 70$ mm, the temperature gradually varied. The temperatures at each point tended to be the same, indicating that the mixing process was complete.

5.3 Temperature-fluctuation intensity changes with height

The position of the maximum temperature-fluctuation intensity on the plate surface evidently changed with height. When $z_p = 30$ mm, an annular shape was observed with a strong temperature fluctuation between the hot and cold fluids. The RMS temperature at the center was relatively low, as shown in Fig. 4b. However, when $z_p = 40$ mm, the RMS temperature above the nozzle showed little difference and only decreased significantly when $r^* > 2$. As the height increased, the RMS temperature gradually decreased, and the temperature-fluctuation intensity at each point gradually became uniform.

The RMS temperature variation in the radial direction are shown in Fig. 6c. The points with higher temperature-fluctuation intensity at different heights are mainly distributed in the circular area above the nozzle in the range $r^* \leq 4$. The temperature-fluctuation intensity is determined by the jet instability and hot and cold fluid mixing with height. As the height increases, the amplitude of the jet sway increases. For low values of height, the point of the most severe temperature fluctuation is between the hot and cold fluids ($r^* = 2$). However, when the height is higher, the intensity of temperature fluctuation in the range of $r^* \leq 4$ tends to be consistent. However, with an increase in the axial direction, the jet mixing becomes more uniform, and the amplitude of the temperature fluctuation decreases gradually. Under the combined action of these two factors, the temperature-fluctuation intensity first increases and then decreases at $r^* = 0$, and it decreases continuously at $r^* = 2$. It remains almost unchanged when $r^* = 6$, as shown in Fig. 6d. This implies that when the plate is located at different heights above the jet, the points affected by the temperature fluctuations that

need to be analyzed are entirely different. When the height is low, the analysis must focus on the locations between the hot and cold-fluid nozzles. When the height is high, a series of positions from the center of the cold-fluid nozzle to the position of the hot fluid nozzle must be comprehensively considered. The analysis of the temperature-fluctuation range in Sect. 5.1 also highlights this phenomenon.

6 Conclusion

In this study, fluid and plate surface temperature fluctuations were experimentally investigated using a setup based on a coaxial-jet model. Essentially, the behavior of the temperature fluctuation of the fluid and the plate surface was studied. Furthermore, the variation in the axial direction was analyzed. The following conclusions were drawn from this study:

- (1) An experimental setup was constructed. The combined standard uncertainty of the temperature measurement is $u_c(T) = 0.311$ K, and the expanded uncertainties of the flow measurement $u_{\text{crels}}(V) = 0.42\text{--}8.4\%$. The setup exhibited sufficient stability and accuracy to study the temperature fluctuations of the fluid and plate surface.
- (2) The temperature fluctuations were mainly caused by the instability of the jet. The instability of the fluid was primarily manifested in the expansion and contraction of the center of the cold fluid over time, the swing of the center position of the jet, and the shape change of the jet. These three factors caused temperature fluctuations on the plate surface. With an increase in the plate height, the jet swing and shape change became more pronounced.
- (3) The dimensionless average temperatures of the fluid and plate surfaces were symmetrical around the center of the cold fluid. For the fluid, it first increased and then decreased along the radial direction; further, it varied linearly along the axial direction within $z_f^* = 0.2\text{--}0.8$. On the plate surface, it increased continuously as the radius increased. It gradually increased at the center with increasing plate height. The average temperature reflects the fluid mixing. Fluid mixes rapidly during $30 < z_p \leq 70$ mm and slowly when $z_p > 70$ mm.
- (4) The maximum temperature-fluctuation intensity on the plate surface was much smaller than that of the fluid. The temperature-fluctuation attenuation was rapid near the surface of the plate. The intensity of the temperature fluctuation on the plate surface was affected by its radius and height. It first increased and then decreased at $r^* = 0$, whereas it continuously decreased at $r^* = 2$ and remained unchanged at $r^* = 6$ as the plate height

increased. When the plate height was low ($z_p < 30$ mm), the analysis should focus on the locations between the hot- and cold fluid nozzles. When the height is high ($z_p > 40$ mm), a series of positions from the center of the cold-fluid nozzle to the hot fluid nozzle must be comprehensively considered.

Author contributions All authors contributed to the study conception and design. Material preparation, data collection and analysis were performed by Xue-Yao Xiong, Zun-Quan Liu and Guo-Yan Zhou. Xing Luo provided experimental suggestions. Shan-Tung Tu provided fund support. The first draft of the manuscript was written by Xue-Yao Xiong, and all authors commented on previous versions of the manuscript. All authors read and approved the final manuscript.

Data availability The data that support the findings of this study are openly available in Science Data Bank at <https://cstr.cn/31253.11.scien.cedb.j00186.00381> and <https://doi.org/https://doi.org/10.57760/scien.cedb.j00186.00381>.

Declarations

Conflict of interest The authors declare that they have no competing interests.

References

1. Y. Lejeail, N. Kasahara, Thermal fatigue evaluation of cylinders and plates subjected to fluid temperature fluctuations. *Int. J. Fatigue* **27**, 768–772 (2005). <https://doi.org/10.1016/j.ijfatigue.2005.01.007>
2. N. Kasahara, H. Takasho, A. Yacumpai, Structural response function approach for evaluation of thermal striping phenomena. *Nucl. Eng. Des.* **212**, 281–292 (2002). [https://doi.org/10.1016/S0029-5493\(01\)00493-9](https://doi.org/10.1016/S0029-5493(01)00493-9)
3. R. Wisler, S.E. Bays, S.J. Yoon, Thermal-striping analysis methodology for sodium-cooled reactor design. *Int. J. Heat Mass Transf.* **175**, 121321 (2021). <https://doi.org/10.1016/j.ijheatmasstransfer.2021.121321>
4. T. Lu, B. Liu, P.X. Jiang, Inverse estimation of the inner wall temperature fluctuations in a pipe elbow. *Appl. Therm. Eng.* **31**, 1976–1982 (2011). <https://doi.org/10.1016/j.applthermaleng.2011.03.002>
5. K. Miyoshi, M. Kamaya, Y. Utanohara et al., An investigation of thermal stress characteristics by wall temperature measurements at a mixing tee. *Nucl. Eng. Des.* **298**, 109–120 (2016). <https://doi.org/10.1016/j.nucengdes.2015.12.004>
6. J. Ahmad, J. Purbolaksono, L.C. Beng, Thermal fatigue and corrosion fatigue in heat recovery wall area side tubes. *Eng. Fail. Anal.* **17**, 334–343 (2010). <https://doi.org/10.1016/j.engfailanal.2009.06.014>
7. A. Tokuhiro, N. Kimura, An experimental investigation on thermal striping: Mixing phenomena of a vertical non-buoyant jet with two adjacent buoyant jets as measured by ultrasound Doppler velocimetry. *Nucl. Eng. Des.* **188**, 49–73 (1999). [https://doi.org/10.1016/S0029-5493\(99\)00006-0](https://doi.org/10.1016/S0029-5493(99)00006-0)
8. Z.Z. Nan, M.Z. Gu, Y.R. Li et al., Effects of the incident angle of branch pipe on the thermal mixing of impinging jets in T-junctions. *Int. J. Heat Mass Transf.* **185**, 122433 (2022). <https://doi.org/10.1016/j.ijheatmasstransfer.2021.122433>
9. M. Bergagio, R. Thiele, H. Anglart, Analysis of temperature fluctuations caused by mixing of non-isothermal water streams at elevated pressure. *Int. J. Heat Mass Transf.* **104**, 979–992 (2017). <https://doi.org/10.1016/j.ijheatmasstransfer.2016.08.082>
10. G.Y. Chuang, Y.M. Ferng, Investigating effects of injection angles and velocity ratios on thermal-hydraulic behavior and thermal striping in a T-junction. *Int. J. Therm. Sci.* **126**, 74–81 (2018). <https://doi.org/10.1016/j.ijthermalsci.2017.12.016>
11. N. Kimura, H. Ogawa, H. Kamide, Experimental study on fluid mixing phenomena in T-pipe junction with upstream elbow. *Nucl. Eng. Des.* **240**, 3055–3066 (2010). <https://doi.org/10.1016/j.nucengdes.2010.05.019>
12. M. Zhou, R. Kulenovic, E. Laurien, Experimental investigation on the thermal mixing characteristics at a 90° T-Junction with varied temperature differences. *Appl. Therm. Eng.* **128**, 1359–1371 (2018). <https://doi.org/10.1016/j.applthermaleng.2017.09.118>
13. C. Walker, M. Simiano, R. Zboray et al., Investigations on mixing phenomena in single-phase flow in a T-junction geometry. *Nucl. Eng. Des.* **239**, 116–126 (2009). <https://doi.org/10.1016/j.nucengdes.2008.09.003>
14. J. Kickhofel, V. Valori, H.M. Prasser, Turbulent penetration in T-junction branch lines with leakage flow. *Nucl. Eng. Des.* **276**, 43–53 (2014). <https://doi.org/10.1016/j.nucengdes.2014.05.002>
15. M. Benyamina, P. Knyazkov, O. Imine, Large eddy simulation of thermal turbulent mixing and reduction of temperature fluctuations with swirl in T-junction. *J. Braz. Soc. Mech. Sci.* **39**, 4985–4999 (2017). <https://doi.org/10.1007/s40430-017-0849-y>
16. Y. Utanohara, A. Nakamura, K. Miyoshi et al., Numerical simulation of long-period fluid temperature fluctuation at a mixing tee for the thermal fatigue problem. *Nucl. Eng. Des.* **305**, 639–652 (2016). <https://doi.org/10.1016/j.nucengdes.2016.06.024>
17. S.X. Qian, N. Kasahara, Large eddy simulation analysis of fluid temperature fluctuations at a T-junction for prediction of thermal loading. *J. Press. Vessel. Technol.* **137**, 011303 (2015). <https://doi.org/10.1115/1.4028067>
18. Z.C. Guo, T. Lu, B. Liu, Inverse heat conduction estimation of inner wall temperature fluctuations under turbulent penetration. *J. Therm. Sci.* **26**, 160–165 (2017). <https://doi.org/10.1007/s11630-017-0925-8>
19. A. Timperi, Conjugate heat transfer LES of thermal mixing in a T-junction. *Nucl. Eng. Des.* **273**, 483–496 (2014). <https://doi.org/10.1016/j.nucengdes.2014.02.031>
20. Y. Utanohara, K. Miyoshi, A. Nakamura, Conjugate numerical simulation of wall temperature fluctuation at a T-junction pipe. *Mech. Eng. J.* **5**(18), 44–00044 (2018). <https://doi.org/10.1299/mej.18-00044>
21. W.Q. Zhuo, F.L. Niu, J.C. Cai et al., Influence of injection temperature and flow rate on mixing and stratification in small passive cooling enclosures. *Nucl. Sci. Tech.* **27**, 91 (2016). <https://doi.org/10.1007/s41365-016-0078-6>
22. M. Dougdag, R. Fernandez, D. Lamberts, Risk assessment of thermal striping in MYRRHA research reactor. *Nucl. Eng. Des.* **319**, 40–47 (2017). <https://doi.org/10.1016/j.nucengdes.2017.04.031>
23. M. Wakamatsu, H. Nei, K. Hashiguchi, Attenuation of temperature fluctuations in thermal striping. *J. Nucl. Sci. Technol.* **32**, 752–762 (1995). <https://doi.org/10.1080/18811248.1995.9731770>
24. S. Chacko, Y.M. Chung, S.K. Choi et al., Large-eddy simulation of thermal striping in unsteady non-isothermal triple jet. *Int. J. Heat Mass Transf.* **54**, 4400–4409 (2011). <https://doi.org/10.1016/j.ijheatmasstransfer.2011.05.002>
25. L.Z. Wang, Y.Q. Bai, M. Jin et al., Comparison analysis of temperature fluctuations for double jet of liquid metal cooled fast reactor. *Ann. Nucl. Energy* **94**, 802–807 (2016). <https://doi.org/10.1016/j.anucene.2016.04.042>

26. L.Z. Wang, G.W. Wu, J. Wang et al., Numerical investigation of the core outlet temperature fluctuation for the lead-based reactor. *Ann. Nucl. Energy* **117**, 194–201 (2018). <https://doi.org/10.1016/j.anucene.2018.03.020>
27. Y.Q. Yu, E. Merzari, J.W. Thomas et al., Steady and unsteady calculations on thermal striping phenomena in triple-parallel jet. *Nucl. Eng. Des.* **312**, 429–437 (2017). <https://doi.org/10.1016/j.nucengdes.2016.06.015>
28. S. Lomperski, A. Obabko, E. Merzari et al., Jet stability and wall impingement flow field in a thermal striping experiment. *Int. J. Heat Mass Transf.* **115**, 1125–1136 (2017). <https://doi.org/10.1016/j.ijheatmasstransfer.2017.07.076>
29. R. Krishna Chandran, G. Padmakumar et al., Numerical analysis of thermal striping phenomena using a two jet water model. *Eng. Appl. Comp. Fluid.* **4**, 209–221 (2014). <https://doi.org/10.1080/19942060.2010.11015311>
30. N. Kimura, H. Miyakoshi, H. Kamide, Experimental investigation on transfer characteristics of temperature fluctuation from liquid sodium to wall in parallel triple-jet. *Int. J. Heat Mass Transf.* **50**, 2024–2036 (2007). <https://doi.org/10.1016/j.ijheatmasstransfer.2006.09.030>
31. Q. Cao, H.Y. Li, D.G. Lu et al., Temperature fluctuation caused by coaxial-jet flow: experiments on the effect of the velocity ratio $R \geq 1$. *Nucl. Eng. Des.* **314**, 142–149 (2017). <https://doi.org/10.1016/j.nucengdes.2017.01.021>
32. D.G. Lu, Q. Cao, J. Lv et al., Experimental study on three-dimensional temperature fluctuation caused by coaxial-jet flows. *Nucl. Eng. Des.* **243**, 234–242 (2012). <https://doi.org/10.1016/j.nucengdes.2011.11.017>
33. B. Kok, Y. Varol, H. Ayhan et al., Experimental and computational analysis of thermal mixing characteristics of a coaxial jet. *Exp. Therm. Fluid Sci.* **82**, 276–286 (2017). <https://doi.org/10.1016/j.expthermflusci.2016.11.028>
34. D. Tenchine, S. Vandroux, V. Barthel et al., Experimental and numerical studies on mixing jets for sodium cooled fast reactors. *Nucl. Eng. Des.* **263**, 263–272 (2013). <https://doi.org/10.1016/j.nucengdes.2013.06.001>
35. B.N. Taylor, C.E. Kuyatt, *Guidelines for evaluating and expressing the uncertainty of NIST measurement results* (National Institute of Standards and Technology, UK, 1994)

Springer Nature or its licensor (e.g. a society or other partner) holds exclusive rights to this article under a publishing agreement with the author(s) or other rightsholder(s); author self-archiving of the accepted manuscript version of this article is solely governed by the terms of such publishing agreement and applicable law.